Effect of Chain Length and Unsaturation on Elasticity of Lipid Bilayers

W. Rawicz,* K. C. Olbrich,† T. McIntosh,‡ D. Needham,† and E. Evans*§

§Department of Physics, University of British Columbia, Vancouver, British Columbia V6T 1Z1, Canada; *Department of Pathology, University of British Columbia, Vancouver, British Columbia V6T 1W5, Canada; ‡Department of Cell Biology, Duke University School of Medicine, Durham, North Carolina 27710 USA; and †Department of Mechanical Engineering and Materials Science, Duke University, Durham, North Carolina 27708 USA

ABSTRACT Micropipette pressurization of giant bilayer vesicles was used to measure both elastic bending k_c and area stretch K_A moduli of fluid-phase phosphatidylcholine (PC) membranes. Twelve diacyl PCs were chosen: eight with two 18 carbon chains and degrees of unsaturation from one double bond (C18:1/0, C18:0/1) to six double bonds per lipid (diC18:3), two with short saturated carbon chains (diC13:0, diC14:0), and two with long unsaturated carbon chains (diC20:4, diC22:1). Bending moduli were derived from measurements of apparent expansion in vesicle surface area under very low tensions (0.001–0.5 mN/m), which is dominated by smoothing of thermal bending undulations. Area stretch moduli were obtained from measurements of vesicle surface expansion under high tensions (>0.5 mN/m), which involve an increase in area per molecule and a small—but important—contribution from smoothing of residual thermal undulations. The direct stretch moduli varied little ($< \pm 10\%$) with either chain unsaturation or length about a mean of 243 mN/m. On the other hand, the bending moduli of saturated/monounsaturated chain PCs increased progressively with chain length from 0.56×10^{-19} J for diC13:0 to 1.2×10^{-19} J for diC22:1. However, quite unexpectedly for longer chains, the bending moduli dropped precipitously to $\sim 0.4 \times 10^{-19}$ J when two or more *cis* double bonds were present in a chain (C18:0/2, diC18:2, diC18:3, diC20:4). Given nearly constant area stretch moduli, the variations in bending rigidity with chain length and polyunsaturation implied significant variations in thickness. To test this hypothesis, peak-to-peak headgroup thicknesses h_{pp} of bilayers were obtained from x-ray diffraction of multibilayer arrays at controlled relative humidities. For saturated/monounsaturated chain bilayers, the distances h_{pp} increased smoothly from diC13:0 to diC22:1 as expected. Moreover, the distances and elastic properties correlated well with a polymer brush model of the bilayer that specifies that the elastic ratio $(k_c/K_A)^{1/2} = (h_{pp} - h_o)/24$, where $h_o \approx 1$ nm accounts for separation of the headgroup peaks from the deformable hydrocarbon region. However, the elastic ratios and thicknesses for diC18:2, diC18:3, and diC20:4 fell into a distinct group below the correlation, which showed that poly-*cis* unsaturated chain bilayers are thinner and more flexible than saturated/monounsaturated chain bilayers.

INTRODUCTION

Most phospholipid acyl chains in animal cell membranes are saturated (only C-C bonds) or monounsaturated (one C═C bond) hydrocarbon polymers. However, it is surprising that membranes rich in polyunsaturated (multiple methylene-interrupted C═C bonds) lipids are found in certain animal tissues (like the brain, for instance), and the lengths of unsaturated lipid chains vary significantly. An obvious question to be asked is, how do hydrocarbon chain unsaturation and length affect membrane material properties important to the function and survival of cells? To address this question, we have used micropipette aspiration methods to test mechanical properties of giant-single bilayer vesicles made from fluid diacyl phosphatidylcholine (PC) bilayers with chain lengths of 13–22 carbons and a wide range of unsaturation (one, two, four, or six double bonds per lipid). Here we report results for equilibrium properties—elastic area and bending moduli. In a companion article (Olbrich et al., 2000), we present results for dynamic properties—rupture strength (lysis tension) and water permeability—for the diC18 lipids with one to six *cis* double bonds. In both studies, major effects of unsaturation were found to occur when two or more *cis* double bonds punctuated by saturated bonds (C═C-C═C) appear in one or both chains. In the case of elasticity, the surprising outcome is that this type of poly-*cis* unsaturation leads to a precipitous reduction in the bending stiffness of the bilayer, which is accompanied by a prominent reduction in thickness, whereas neither chain length nor unsaturation significantly affects lateral area compressibility.

Several techniques have been used to quantitate mechanical stretch properties of bilayers. Most prominent are the micropipette approach we have pioneered for giant vesicles (Kwok and Evans, 1981; Evans and Needham, 1987), photon correlation spectroscopy and dynamic light scattering of small vesicles under osmotic stress (Rutkowski et al., 1991; Hallett et al., 1993), cryoelectron microscopy of vesicles subjected to osmotic stress (Mui et al., 1993), and NMR and x-ray diffraction of strongly dehydrated multibilayer arrays (Koenig et al., 1997). Of these approaches, only the micropipette method can be used to test the expansion of a single bilayer with a resolution of better than 0.1% relative change in area and verify elastic reversibility. In contrast to area stretch properties, the small bending stiffness of a bilayer has been derived traditionally from a detailed analysis of thermal shape fluctuations of flaccid vesicles

Received for publication 1 October 1999 and in final form 28 March 2000.

Address reprint requests to Dr. Evan A. Evans, Department of Physics, University of British Columbia, Vancouver, BC V6T 1Z1, Canada. Tel.: 604-822-7103; Fax: 604-822-7635; E-mail: evans@physics.ubc.ca.

0006-3495/00/07/328/12 $2.00

(Schneider et al., 1984; Duwe et al., 1987; Faucon et al., 1989; and others) and more recently by measurement of the forces needed to pull nanoscale bilayer tubes from vesicles under tension (Bo and Waugh, 1989; Evans and Yeung, 1994; Evans et al., 1996). Much less complicated, however, is the micropipette pressurization of a single vesicle, which can also be used to quantitate the bilayer bending modulus. The approach is to measure the entropy-driven tension that arises as thermal bending undulations are smoothed under pipette pressurization of a giant vesicle (Evans and Rawicz, 1990, 1997). In the work reported here, both bending and elastic area stretch properties of the PC bilayers have been obtained by the micropipette pressurization technique.

MATERIALS AND METHODS

Lipids

Twelve synthetic species of diacyl-PC lipids were obtained from Avanti Polar Lipids (Alabaster, AL) in chloroform and used without further purification. Nine were *cis* unsaturated: 1-stearoyl-2-oleoyl-sn-glycero-3-phosphocholine (C18:0/1_{c9}); 1-oleoyl-2-stearoyl-sn-glycero-3-phosphocholine (C18:1_{c9}/0); 1,2-dipetroselinoleoyl-sn-glycero-3-phosphocholine (diC18:1_{c6}); 1,2-dioleoyl-sn-glycero-3-phosphocholine (diC18:1_{c9}); 1-stearoyl-2-linoleoyl-sn-glycero-3-phosphocholine (C18:0/$2_{c9,12}$); 1,2-dilinoleoyl-sn-glycero-3-phosphocholine (diC18:$2_{c9,12}$); 1,2-dilinolenoyl-sn-glycero-3-phosphatidylcholine (diC18:$3_{c9,12,15}$); 1,2-diarachidonoyl-sn-glycero-3-phosphocholine (diC20:$4_{c5,8,11,14}$); and 1,2-dierucoyl-sn- glycero-3-phosphocholine (diC22:1_{c13}). One was *trans*-unsaturated: 1,2-elaidoyl-sn-glycero-3-phosphocholine (diC18:1_{t9}). Two were fully saturated: 1,2-ditridecanoyl-sn-glycero-3-phosphocholine (diC13:0) and 1,2-dimyristoyl-sn-glycero-3-phosphocholine (diC14:0). The solutions were placed in amber glass screw-cap vials with Teflon-lined silicone septa. The vials were wrapped in aluminum foil and stored at −20°C under argon, which was especially important for the preservation of lipids containing oxidation-prone fatty acid chains (18:0/2, 18:2, 18:3, 20:4).

Vesicle preparation and lipid oxidation assay

In our laboratories, the generic procedure for preparation of giant vesicles (15–30-μm diameter) is to rehydrate lipid films dried first from chloroform:methanol (2:1) onto the surface of a roughened Teflon disk (Needham et al., 1988). After deposition of the lipid film and evaporation of the organic solvent in vacuo, the Teflon disk is covered with a warm (37°C) sucrose solution (200 mOsm) and allowed to hydrate. To create a refractive index contrast between the inside and outside of vesicles and to sediment vesicles in the microscope chamber, an aliquot of vesicles is diluted manyfold in an equiosmolar solution of glucose or electrolyte buffer. The refractive index gradient is used to enhance optical detection of the projection length, as shown by the example in Fig. 1. Described below, accurate video tracking of the edge enables discrimination of $<0.1\%$ relative change in vesicle area or volume, even though optical measurements of total area and volume remain limited to an accuracy of a few percent by diffraction. For the formation of vesicles from polyunsaturated lipids, slight modifications were made in the procedure. First, argon-purged, deionized water was used to make the hydration and suspension solutions. Second, the container with the polyunsaturated lipid film was wrapped in aluminum foil (to minimize exposure to light). The polyunsaturated lipids were allowed to hydrate for only 3 h under argon and were used immediately (normally, lipids are left to hydrate overnight and then used the next day). In the initial phase of the study, samples of the polyunsaturated lipids were tested for possible oxidative damage over the time scales associated with preparation and experiment by spectrophotometric assay (Kim and LaBella, 1987; New, 1990). The absorbance of a solution of 1 mM lipid in absolute ethanol was measured at ~230 nm with a Beckman DU-7500 diode array spectrophotometer (Beckman, Fullerton, CA). Absorption at this wavelength indicates the presence of conjugated dienes in the hydrocarbon chain, which result from oxidation (Kim and LaBella, 1987; New, 1990). Lipid samples used soon after arrival from Avanti showed no detectable oxidative damage. Moreover, measurements of properties repeated with preparations from the same polyunsaturated lipid samples and those from new samples purchased at later times gave identical results.

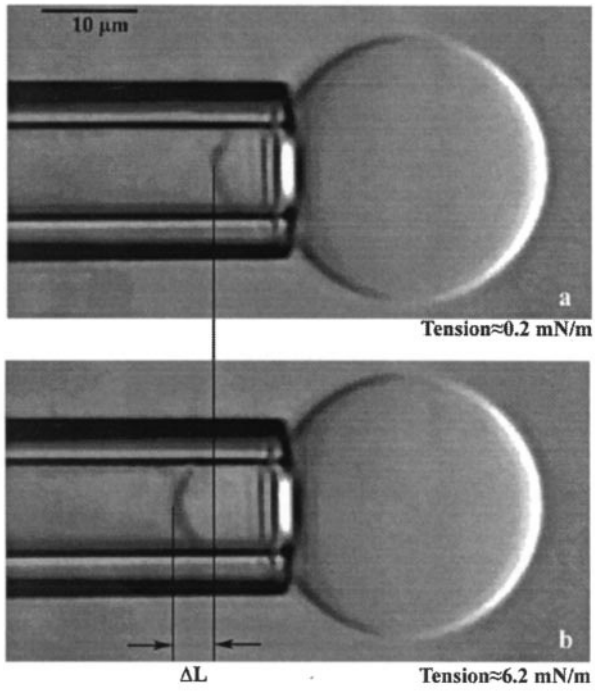

FIGURE 1 Video micrograph of a vesicle area expansion test. (*a*) The vesicle at low tension. (*b*) The vesicle at high tension. The change in projection length ΔL_p is proportional to the change in apparent surface area ΔA.

Mechanical expansion of apparent vesicle area

Micropipette suction was used to pressurize vesicles and test elastic area expansion. Well established from mechanics (Kwok and Evans, 1981), the suction pressure P applied to a fluid bilayer vesicle produces a uniform membrane tension τ_m, which is described by a geometric relation based on the pipet caliber (diameter) D_p and diameter D_v of the vesicle spherical segment exterior to the pipette, i.e.,

$$\tau_m = PD_p/4(1 - D_p/D_v)$$

The pipette suction (~10^3 Pa) needed to expand the surface of a ~20-μm vesicle is small compared to osmotic driving forces (~10^5 Pa) required to kinetically displace water on the time scale of the experiment and small compared to the osmotic activity of the trapped sucrose (~5×10^5 Pa). Thus vesicle volume remains effectively fixed in an area expansion test. Movement of the projection length L_p inside the pipette provides a direct measure of the area increase. Using measurements of the vesicle spherical segment and cylindrical projection dimensions, we computed precise changes in apparent area ΔA numerically for each displacement ΔL_p of the

projection length with simple geometric formulae and the constraint of a fixed vesicle volume (see the Appendix in Olbrich et al., 2000). The proportionality between apparent area and length is easily seen in the following first-order approximation:

$$\Delta A \approx \pi D_p(1 - D_p/D_v)\Delta L_p$$

Displacement of the projection length of an aspirated vesicle under change in suction pressure is shown in Fig. 1. Even though apparent area can be measured over a tension range from 10^{-3} mN/m to vesicle rupture (~ 3–10 mN/m) as shown in Fig. 2, vesicle area expansion was examined in two separate regimes of low and high tension to minimize the duration of experiments and thereby avoid any reduction in vesicle volume caused by chamber dehydration at long times.

In the low-tension regime (0.001–0.5 mN/m), the vesicle surface increases by smoothing of subvisible thermal shape fluctuations (bending undulations). Even though a vesicle looks perfectly spherical in optical images under suction pressures of ~0.1 Pa or more (cf. Fig. 1), thermal shape fluctuations persist on the suboptical scale and act as a small reservoir for an increase in apparent surface area of the vesicle. To examine the low-tension regime, each vesicle was first prestressed under a tension of ~0.5 mN/m to ensure that small hidden projections of bilayer surface were pulled into the surface. After the vesicle was prestressed, suction pressures were dropped to ~0.1 Pa, which lowered the bilayer tension to 10^{-3} mN/m. Then suction was increased in steps—each held steady for several seconds—up to 2–3 × 10^2 Pa, where tensions approached 1 mN/m. Finally, a stepwise course of pressure reduction was used to verify reversibility. As shown by the data in Fig. 2 *A*, bilayer tension below ~0.5 mN/m increases as a very weak exponential of apparent area, which is verified by the linear increase in apparent area with log(tension) in Fig. 2 *B*. Tests of bending elasticity in the low-tension regime for the diC18 PCs were performed at 18°C (close to the dewpoint) to minimize chamber dehydration and to allow long working periods without having to change chamber solutions. But bending tests for diC13:0, diC14:0, and diC22:1 PC were performed at 22°C, 29°C, and 21°C, respectively, to be well separated from the main liquid crystal-crystalline phase transition. Measurements at high temperatures (lower relative humidities) are usually no problem but require more frequent sample changes to avoid chamber dehydration.

In the high-tension regime (>0.5 mN/m), direct surface stretch or dilation in area per lipid molecule becomes significant with a small, diminishing contribution from smoothing of thermal undulations. To examine the high-tension regime, each vesicle was first prestressed under a tension of ~0.5 mN/m to incorporate hidden excess area, and then suction was increased in steps—each held steady for several seconds—up to a sublytic threshold of 1–3 × 10^3 Pa, where tensions reached 3–8 mN/m. As before, a stepwise course of pressure reduction was used to verify reversibility. As shown by the data in Fig. 2 *A*, bilayer tension seems to increase in direct proportion to apparent area above ~1 mN/m but with different slopes for two different types of lipid bilayers. Much shorter in duration than the low-tension experiments, all area compressibility tests in the high-tension regime were performed at 21°C.

Bilayer thickness

X-ray diffraction was performed on oriented lipid multibilayers of six lipids by methods described previously (see McIntosh, 1987; McIntosh et

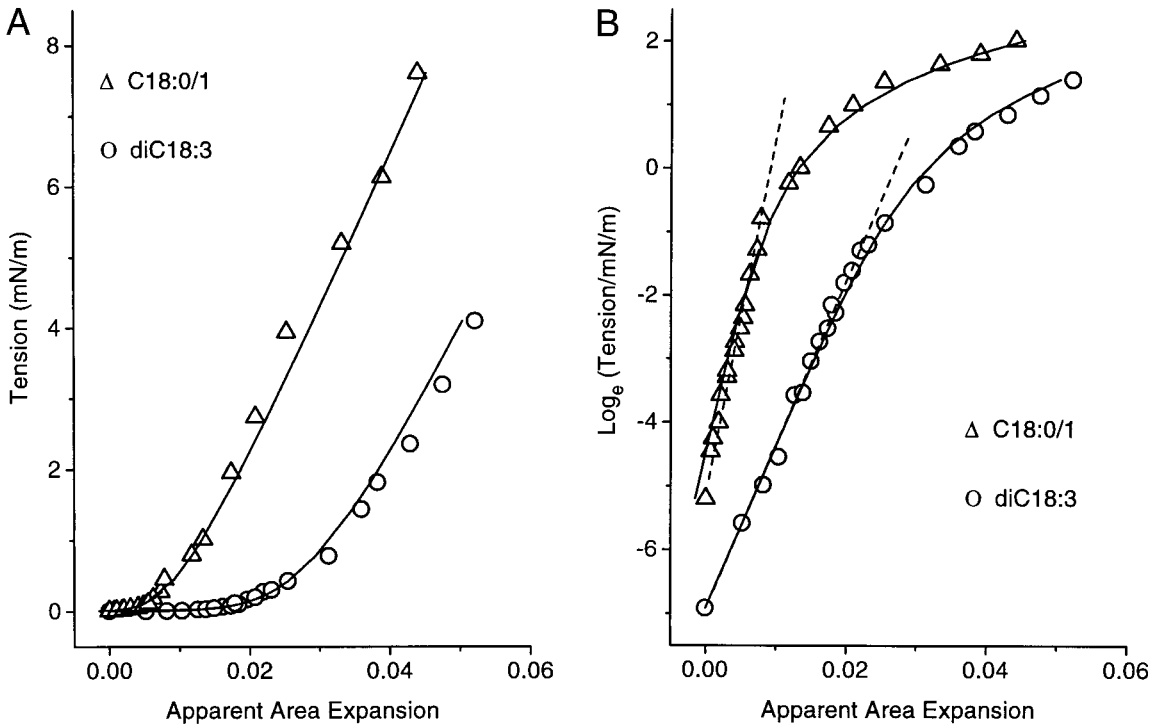

FIGURE 2 Examples of apparent area expansion measured over tensions from 0.001 to 8 mN/m for two vesicles made from C18:0/1 and diC18:3 PC. (*A*) Linear plot of tension versus apparent area expansion. The initial soft-exponential rise of tension with area expansion reveals smoothing of thermal shape fluctuations, which is followed by the onset of linear increase in tension as the bilayer begins to stretch. (*B*) Semilog plot of tension versus apparent area expansion. Slopes of the linear fits (*dashed lines*) applied to the range of very low tensions yield elastic bending moduli k_c (× $8\pi/k_BT$) for each bilayer (k_c = 0.9 × 10^{-19} J for C18:0/1 and k_c = 0.4 × 10^{-19} J for diC18:3). The solid curves in *A* and *B* are the fit of the elastic compressibility relation (Eq. 1) over the entire four-order-of-magnitude range of tension, using the values of bending elasticity and a common value of the direct expansion modulus (K_A = 230 mN/m) for both lipid vesicles.

al., 1989, 1992, for details). Partially hydrated, oriented bilayers of diC13:0, C18:0/1, diC18:1, diC18:2, diC18:3, and diC22:1 PC were formed by first placing a drop of lipid/chloroform solution on a curved glass support, slowly evaporating the chloroform, and then incubating the multilayers in a constant-humidity atmosphere. Afterward, the specimen was placed in a controlled humidity chamber on a single-mirror (line-focused) x-ray camera so that the x-ray beam was oriented at a grazing angle with respect to the multilayers. The relative humidity in the chamber was maintained at 98%, 93%, or 79% relative humidity with a cup of the appropriate saturated salt solution (McIntosh, 1987; McIntosh et al., 1989). To speed equilibration, a gentle stream of nitrogen gas was passed through a flask of the saturated salt and then through the chamber.

X-ray diffraction patterns were recorded at ambient temperatures on a stack of six sheets of Kodak DEF x-ray film loaded in a flat plate film cassette. After background subtraction, integrated intensities $I(n)$ were obtained for each order n by measuring the area under each diffraction peak. The intensities of the oriented line-focused patterns were corrected by a single factor of n due to the cylindrical curvature of the multilayers (Blaurock and Worthington, 1966; Herbette et al., 1977), which yields a structure amplitude of $F(n) = \{nI(n)\}^{1/2}$. Then electron density profiles $\rho(x)$ were calculated on a relative scale from the Fourier transform,

$$\rho(x) = (2/d)\Sigma_n \exp\{i\phi(n)\} \cdot F(n) \cdot \cos(2\pi nx/d)$$

where x is the distance from the center of the bilayer, d is the lamellar repeat period, $\phi(n)$ is the phase angle for order n, and the sum Σ_n is over n. Phase angles were determined using the sampling theorem (Shannon, 1949) as described previously (McIntosh and Simon, 1986; McIntosh, 1987). Fig. 3 demonstrates typical structure factors for C18:0/1 and diC18:3, along with continuous Fourier transforms calculated using the sampling theorem. The resolution of the electron density profiles presented in this paper is $d/2h_{max} \approx 7$ Å. However, as shown previously by McIntosh and Simon (1986), Nagle et al. (1996), and Petrache et al. (1998b), profiles with 7-Å resolution provide a quite accurate estimate ($\leq$ Å) for the peak-to-peak headgroup separation across the bilayer. The critical requirement is that the profiles for all of the lipid measurements are obtained at the same resolution.

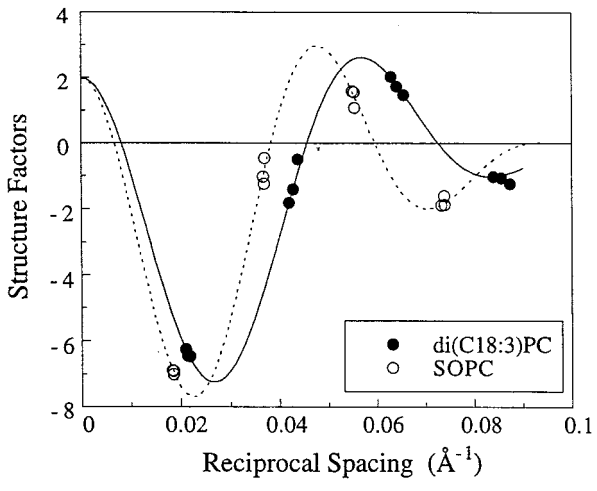

FIGURE 3 Examples of structure factors and continuous Fourier transforms obtained by x-ray diffraction from C18:0/1 (○) and diC18:3 (●) multibilayers.

RESULTS

Measurements of bilayer elastic properties

As described above, measurements of aspiration length versus pipette pressurization were converted to apparent area expansion versus tension properties of bilayer vesicles in low- and high-tension regimes. Verified as reversible, the tension-apparent area results were correlated with a general constitutive relation for elastic dilation of fluid bilayers to obtain the direct lipid area expansion and bending moduli. Based on early concepts of Helfrich (Helfrich and Servuss, 1984), apparent area compressibility is derived from a superposition of smoothing of thermal bending undulations and reduction in lipid surface density (Evans and Rawicz, 1990, 1997),

$$\alpha = (k_BT/8\pi k_c)\ln(1 + c\tau_m A/k_c) + \tau_m/K_A \qquad (1)$$

$\alpha = \Delta A/A_o$ is the fractional increase in apparent or mean projected area A of the vesicle; K_A, k_c are the elastic moduli for direct stretch in area and for bilayer bending, respectively; thermal energy k_BT is $\sim 4 \times 10^{-21}$ J; c is an unimportant constant of ~ 0.1 that depends on the type of modes (spherical harmonics or plane waves) used to describe surface undulations. Fig. 2 shows the correlation of Eq. 1 with measurements of apparent area for two different types of lipid vesicles over the full range of accessible tensions. In the soft-thermal regime at low tension, the apparent expansion relative to an initial state of tension $\tau_m(0)$ is dominated by smoothing of thermal undulations, and the bending stiffness is revealed by the logarithmic dependence of apparent area on tension, $\log_e[\tau_m/\tau_m(0)] \approx (8\pi k_c/k_BT)\Delta A/A_o$, as derived from the dashed line fits in Fig. 2 *B*. By comparison at high tension, an increase in apparent area approaches the direct stretch $\Delta A'/A'_o$, governed by the elastic area-stretch modulus, which increases linearly with tension, $\tau_m = K_A(\Delta A'/A'_o)$. Even so, residual thermal undulations introduce a small (but important) correction in the high-tension regime, as revealed by the slight curvature in the high-tension results of Fig. 2 *A*.

Bending moduli

Because of the logarithmic dependence on tension, the apparent expansion of vesicle area had to be measured over a large range of minuscule tensions to obtain the bending modulus. Limited by the 0.1 Pa pressure sensitivity, the regime of low tension accessible to pipette aspiration spanned nearly three orders of magnitude from 10^{-3} to ~ 0.5 mN/m. Seen in Fig. 2 *B*, vesicle areas increase linearly with log(tension) over most of this range. Multiplied by $k_BT/8\pi \approx 1.6 \times 10^{-22}$ J or $0.04k_BT$, the slope of $\log_e$(tension) versus fractional area expansion in the low-tension regime yielded the bending modulus of a bilayer as demonstrated by the dotted line fits to the data in Fig. 2 *B*. Tests

of at least 10 vesicles were used to obtain bending moduli for each type of lipid as listed in Table 1 (± SD). The bending moduli of saturated/monounsaturated PCs increased progressively with chain length from $k_c = 0.56 \times 10^{-19}$ J ($\approx 14k_BT$) for diC13:0 to $k_c = 1.2 \times 10^{-19}$ J ($\approx 30k_BT$) for diC22:1. But unexpectedly for longer chains, the bending moduli of bilayers with two or more alternating *cis* double bonds along one or both chains (C18:0/2, diC18:2, diC18:3, and diC20:4) dropped precipitously to $k_c \approx 10$–$11k_BT$, which shows that poly-*cis* unsaturated membranes are distinctly more flexible than saturated/monounsaturated PC bilayers. To illustrate the striking effect of polyunsaturation, Fig. 4 presents a histogram of the bending moduli (± SD) for diC18 bilayers arranged in order of increasing unsaturation.

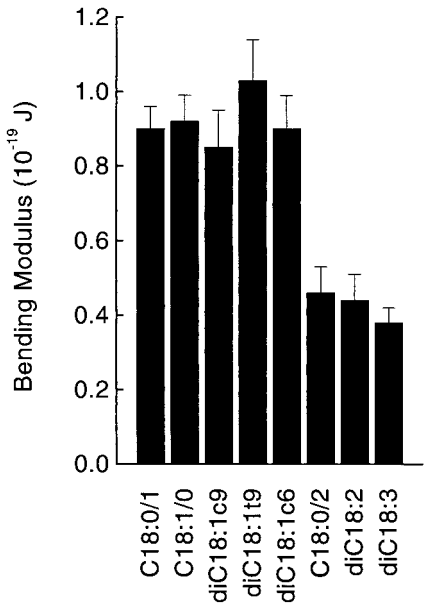

FIGURE 4 Elastic bending moduli for diC18 PC bilayers arranged in order of increasing unsaturation.

Lipid area dilation moduli

Ideally, both bending and direct stretch moduli can be derived from a nonlinear fit of Eq. 1 to measurements of apparent area over the full range of high and low tensions. However, for reasons given above and just as accurately within experimental resolution, the bending modulus can be derived first from the low-tension regime then used with the constitutive Eq. 1 to carry out a one-parameter fit to the apparent area expansion in the high-tension regime (>0.5 mN/m). The result is indistinguishable from the correlation over the full range of tension as demonstrated in Fig. 2. When the value of the bending modulus is known, the contribution to apparent area expansion from smoothing thermal undulations can be determined uniquely in the high-tension regime. For each *i*th data pair of apparent area expansion and tension, the direct area dilation $\alpha'(i) = \alpha(i) + \Delta\alpha(i)$ is found relative to an initial tension state $\tau_m(1)$, using the correction

$$\Delta\alpha(i) = -(k_BT/8\pi k_c)\log_e[\tau_m(i)/\tau_m(1)] \qquad (2)$$

The direct area expansion α' found in this way is plotted versus tension in Fig. 5 for the vesicle tests in Fig. 2. Although the slope K_{app} of tension versus apparent area expansion above 1 mN/m differs significantly between the two lipid bilayers in Fig. 2 *A*, a common value of $K_A = 230$ mN/m was found for the direct stretch modulus—either by fit of the constitutive equation over the full range of data in Fig. 2 or linear regression to the tension versus direct area expansion in Fig. 5.

To obtain direct stretch properties for a population of vesicles, we used the average bending modulus to correct the values of apparent area expansion measured in the high-tension regime (>0.5 mN/m) with Eq. 2. The statistical uncertainty introduced into the determination of direct-stretch moduli due to the ±10% variation in bending modulus ranges from only ±3% for the stiffest bilayers to ±8–10% for the most flexible bilayers, which lies within the experimental standard deviation. Tests were performed on at least 10 vesicles for each type of lipid to obtain values of K_A (± SD), which are listed in Table 1, along with apparent expansion moduli K_{app}. Comparison of K_{app} and K_A demonstrates that the smoothing of thermal undulations is quite significant for highly flexible bilayers. Unlike bending elasticity, the direct-stretch moduli varied little with

TABLE 1 Peak-to-peak headgroup thicknesses h_{pp}, elastic area K_A, K_{app}, and bending k_c moduli for fluid phase bilayers made from phosphatidylcholines

Lipid	h_{pp} (nm)	K_A (mN/m)	K_{app} (mN/m)	k_c (10^{-19} J)
diC13:0	3.41 ± 0.05	239 ± 15	153 ± 13	0.56 ± 0.07
diC14:0	3.52 ± 0.06	234 ± 23	150 ± 14	0.56 ± 0.06
C18:0/1	4.07 ± 0.06	235 ± 14	208 ± 10	0.90 ± 0.06
C18:1/0	—	230 ± 10	207 ± 8	0.92 ± 0.07
diC18:1_{c9}	3.69 ± 0.04	265 ± 18	237 ± 16	0.85 ± 0.10
diC18:1_{t9}	—	229 ± 12	208 ± 10	1.03 ± 0.11
diC18:1_{c6}	—	235 ± 17	209 ± 14	0.90 ± 0.09
C18:0/2	—	241 ± 22	193 ± 17	0.46 ± 0.07
diC18:2	3.49 ± 0.03	247 ± 21	190 ± 18	0.44 ± 0.07
diC18:3	3.43 ± 0.06	244 ± 32	159 ± 19	0.38 ± 0.04
diC20:4	3.44 ± 0.07	250 ± 10	183 ± 8	0.44 ± 0.05
diC22:1	4.37 ± 0.05	263 ± 10	244 ± 8	1.2 ± 0.15

K_{app} are the slopes of tension versus apparent area dilation measured by micropipette pressurization of vesicles in the high-tension regime; K_A are the direct elastic stretch moduli obtained after correction for smoothing of thermal undulations. Peak-to-peak headgroup thicknesses h_{pp} were measured by x-ray diffraction of multibilayers equilibrated at 98% relative humidity. All values are given as mean ± SD. (Thicknesses h_{pp} for dimyristoyl (diC14:0) and diarachidonoyl (diC20:4) PC bilayers are taken from Petrache et al. (1998b) and McIntosh (1995), respectively.)

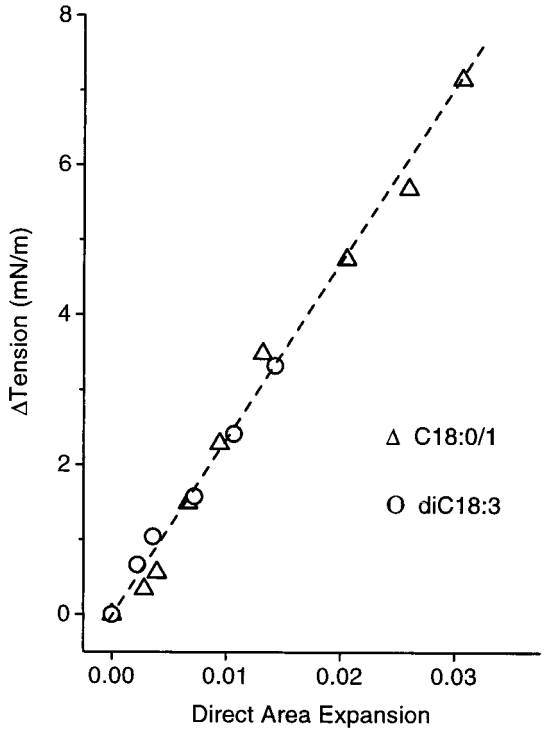

FIGURE 5 The direct area expansion versus increase in tension over the high-tension regime (>0.5 mN/m) for the C18:0/1 and diC18:3 vesicles in Fig. 2. The direct area expansion was obtained from the increase in apparent area, using the correction for smoothing of thermal shape fluctuations (Eq. 2) and mean values of elastic bending moduli measured for each type of lipid bilayer. A common linear regression fits both sets of data and yields the same direct expansion modulus (K_A = 230 mN/m), which matches the result from the fit of the elastic compressibility relation (Eq. 1) over the full four-order-of-magnitude range in tension.

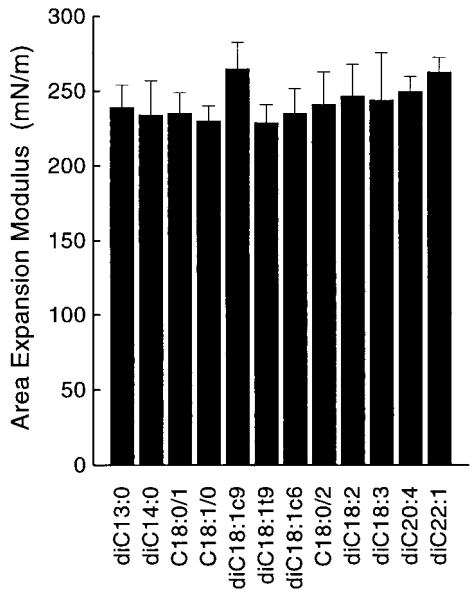

FIGURE 6 Direct area stretch moduli for fluid-phase diacyl PC bilayers with chain lengths from 13 to 22 carbons and range of unsaturation from 0 to 6 double bonds per lipid.

chain unsaturation or length, as shown by the histogram in Fig. 6.

Measurements of bilayer thicknesses

From the mechanics of thin materials it is well known that the bending modulus should scale as the area modulus multiplied by the square of thickness h^2, i.e., $k_c = K_A h^2/c_e$, where c_e is a normalization constant. Thus, because there were small changes in area moduli, we expected that the prominent variations in bending stiffnesses of bilayers were due to differences in bilayer thickness. The explicit prediction is that the elastic ratio $(k_c/K_A)^{1/2}$ should vary linearly with bilayer thickness. Hence by x-ray diffraction, we measured the peak-to-peak headgroup distances h_{pp} for diC13:0, C18:0/1, diC18:1, diC18:2, diC18:3, and diC22:1 PC bilayers, which were combined with distances for diC14:0 and diC20:4 from the literature (Petrache et al., 1998b; McIntosh et al., 1995). For multibilayer arrays held at fixed relative humidity, the x-ray diffraction patterns consisted of four sharp reflections that indexed as orders of a lamellar phase. As demonstrated in Fig. 3 for C18:0/1 and diC18:3, the structure factors obtained from the data closely matched the continuous transforms. The lamellar repeat periods were 54.6 Å, 54.2 Å, and 54.1 Å for C18:0/1 and 47.7 Å, 46.8 A, and 45.8 Å for diC18:3 PC at 98%, 93%, and 79% relative humidity, respectively. The electron density profiles for C18:0/1 and diC18:3 PC at the three relative humidities are shown as examples in Fig. 7, *A* and *B*. The high density peaks in each profile correspond to the lipid headgroups, and the low electron density region in the center of the profile corresponds to the lipid hydrocarbon chains. Note that the general shape of the profiles changed little over this range of relative humidity (and water content); however, the electron density trough was more pronounced in the middle of the bilayer for C18:0/1 than for diC18:3. Thus the low-density terminal methyl groups were localized in the center of the bilayer for C18:0/1, which indicates a more ordered hydrocarbon region than for diC18:3. Differences in thicknesses of C18:0/1 and diC18:3 bilayers are readily appreciated when compared at the same relative humidity (98%) as in Fig. 7 *C*. Analyzing the profiles for the six lipids, we found a progressive increase in the headgroup separation across the bilayer with an increase in the number of carbons and a striking decrease in separation with poly-*cis* double bonds. Listed in Table 1 for 98% relative humidity, the values were $h_{pp} \approx 43.7 \pm 0.5$ Å for diC22:1, $h_{pp} \approx 40.7 \pm 0.6$ Å for C18:0/1, $h_{pp} \approx 36.9 \pm 0.4$ Å for diC18:1, $h_{pp} \approx 34.9 \pm 0.3$ Å for diC18:2, $h_{pp} \approx 34.3 \pm 0.6$ Å for diC18:3, and $h_{pp} \approx 34.1 \pm 0.5$ Å for diC13:0. (As pointed out by Petrache et al. (1998a), measurements of peak-to-peak

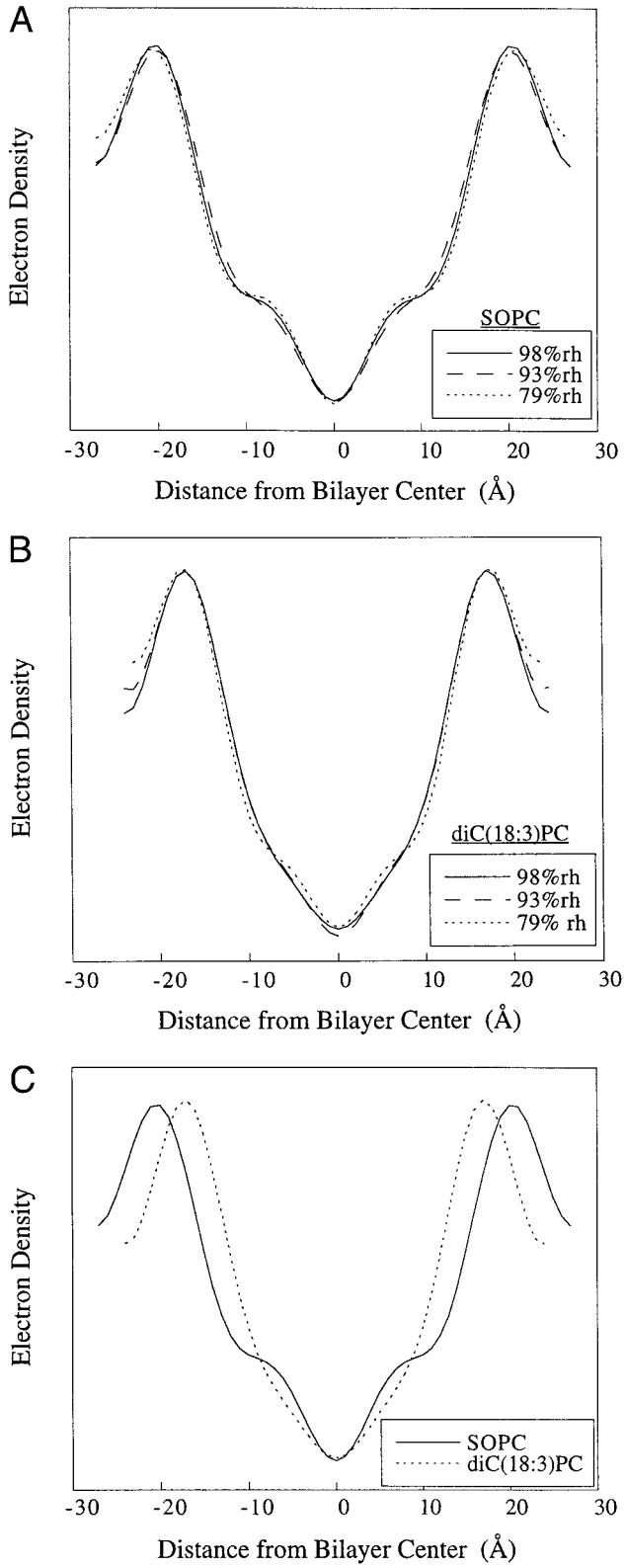

FIGURE 7 Electron density profiles for (*A*) C18:0/1 and (*B*) diC18:3 at 98%, 93%, and 79% relative humidities. (*C*) Electron density profiles of C18:0/1 (*solid line*) and diC18:3 (*dotted line*) compared at 98% relative humidity, which shows the major reduction in peak-to-peak headgroup distance from ~4.1 nm for C18:0/1 to ~3.4 nm for diC18:3.

headgroup separation must also be corrected for thermal bending undulations. However, equilibrated at 98% relative humidity, the multibilayers are squeezed by 20 atm of stress. This level of stress suppresses undulations and limits the corrections to a range from ~ -0.3 Å for diC22:1 to ~ -0.5 Å for diC18:3. The corrections are comparable to the measurement uncertainty and thus are neglected.)

In relating bending stiffness to measurements of structural thickness, it is important to recognize that elastic properties of the membrane are governed by a mechanical thickness h, which depends on the stress distribution across the bilayer. Hence the mechanical thickness will be less than the peak-to-peak headgroup separation by a nondeformable length h_o (i.e., $h = h_{pp} - h_o$) that reflects both the distances of the headgroup peaks from the compact hydrocarbon region and nonuniformity in chain stresses. For a common value of h_o, the ratio $(k_c/K_a)^{1/2}$ should still depend linearly on the peak-to-peak headgroup separation. As a test of this hypothesis, Fig. 8 is a plot of the elastic ratios $(k_c/K_A)^{1/2}$ as a function of the h_{pp} values measured at ~98% relative humidity from Table 1 plus the published values for diC14:0 (Petrache et al., 1998b) and diC20:4 (McIntosh et al., 1995). To provide a specific model for the elastic ratio that reflects lipid structure, we have worked out a simple theory in the Appendix, where each monolayer is viewed as a collection of extended polymer chains held together by hydrophobic interactions at the interface. This polymer

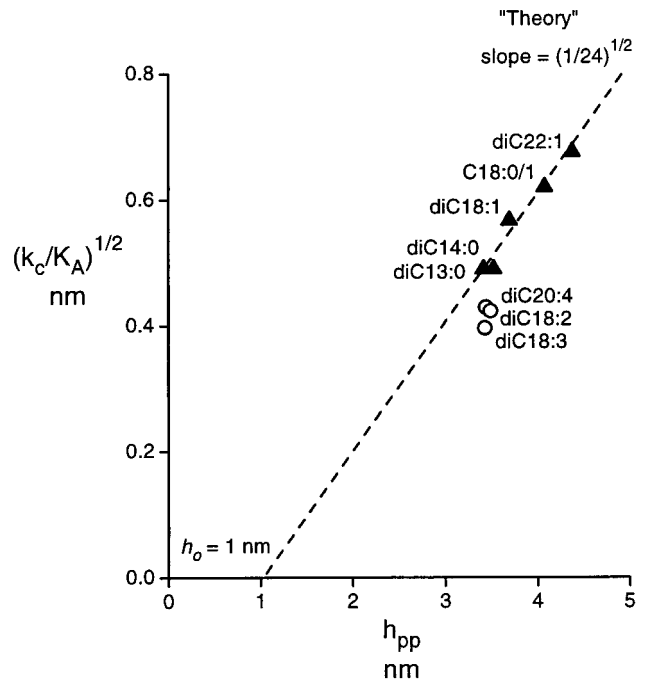

FIGURE 8 Correlation of the elastic ratio $(k_c/K_A)^{1/2}$ for bending:direct stretch with the peak-to-peak headgroup separations h_{pp} taken from Table 1. The solid line is the polymer brush model $(k_c/K_A)^{1/2} = (h_{pp} - h_o)/(24)^{1/2}$ for bilayer elasticity derived in the Appendix, with $h_o = 1$ nm.

brush model predicts that $(k_c/K_A)^{1/2} = (h_{pp} - h_o)/(24)^{1/2}$ and provides a rationale for the minimal variation in the direct-stretch modulus. Over a wide range of chain lengths, the straight line in Fig. 8 shows that the saturated/monounsaturated chain bilayers (diC13:0, diC14:0, C18:0/1, diC18:1, diC22:1PC) correlate well with the polymer brush model fit only by the value of h_o (= 1 nm). Interestingly, however, results for the polyunsaturated bilayers (diC20:4, diC18:2, diC18:3 PC) fall into a distinct group below the correlation. The shift implies that the mechanical thicknesses of these highly unsaturated bilayers would be ~13–15% less than for saturated/monounsaturated chain bilayers.

DISCUSSION

The important outcomes of this work are first that diacyl PC bilayers with a wide range of chain length and unsaturation exhibited little difference in direct area expansion moduli once increases in apparent area were corrected for smoothing of subvisible thermal bending undulations. Second, by comparison, bending rigidity increased in a steady, progressive manner with the number of carbons for saturated/monounsaturated chain bilayers. However, most striking was a major reduction in bending rigidity, which occurred when two or more *cis* double bonds were present in one or both chains of the lipid. Because of the unusual bending flexibility of polyunsaturated chain bilayers, a much larger fraction of surface area is incorporated into thermal undulations, which significantly lowers the apparent area modulus, as seen by comparison of K_A to K_{app} in Table 1. This feature accounts for the ~20–40% variations in elastic area moduli of different PC bilayers published in the past by our groups and others. Recently, for example, Koenig et al. (1997) used NMR and x-ray methods to derive the elastic area moduli for C18:0/1 and diC14:0. Their values were ~220 mN/m and ~140 mN/m for C18:0/1 and diC14:0, respectively, which are consistent with the apparent moduli K_{app} in Table 1 and point to thermal undulations as the source of deviation from the direct-stretch moduli K_A. Finally, measurements of peak-to-peak headgroup separation by x-ray diffraction confirmed the hypothesis that the prominent variations in bending stiffness emanated principally from variations in bilayer thickness. In the case of saturated/monounsaturated chain bilayers, the measurements of the elastic ratio $(k_c/K_A)^{1/2}$ and structural thickness h_{pp} correlated well with the linear prediction obtained from the polymer brush model for bilayer elasticity (Appendix), which implied a fixed length of $h_o = 1$ nm for the combined separations of headgroup centers from the deformable hydrocarbon core. Based on purely geometric considerations and molecular structure, Hitchcock et al. (1974) and McIntosh and Simon (1986) also concluded that $h_o \approx 1$ nm was needed to estimate the thickness of the compact hydrocarbon region and, thereby, obtain the area per lipid $2a$, using the hydrocarbon packing relation $2a \times (h_{pp} - h_o) = 4a_c \times L$. Similarly, Petrache et al. (1998b) arrived at a length of $h_o = 0.82$ nm for dimyristoylphosphatidylcholine. On the other hand, correlation of the elastic ratio to thickness for diC18:2, diC18:3, and diC20:4 PC bilayers showed that poly-*cis* unsaturated chain bilayers are thinner and more flexible than saturated/monounsaturated chain bilayers.

Although naïve in many respects, some useful insights into the origins of bilayer elasticity and thickness are found in the idealized (polymer brush) model of lipid monolayers as structureless polymer chains confined by a constant hydrophobic energy density. First of all, the polymer brush model predicts that the surface pressure Π in each monolayer and the direct expansion modulus of a bilayer are related by a constant factor of 6, i.e., $K_A = 2(3\Pi)$. The numerical factor reflects the inverse cube dependence of surface pressure on area per acyl chain governed by the Gaussian-harmonic regime of polymer extension. In the absence of mechanical tension, the surface pressure in each monolayer is balanced by the interfacial energy density γ for hydrophobic interactions, $\Pi = \gamma$. Consequently, the model predicts that elastic area compressibility is constant if the interfacial energy density γ is constant (per the idealized concept of hydrophobic interactions). Consistent with this prediction, direct-stretch moduli of the 12 PC bilayers vary little in a range of 230–250 mN/m, except for diC18:1_{c9} and diC22:1_{c13} at 263–265 mN/m. As such, the mean value of 243 mN/m implies that monolayer surface pressure varies little from $\gamma \approx 40$ mJ/m^2 (mN/m). The $< \pm 10\%$ variations from 243 mN/m obviously reflect deviations from the idealized model, which could arise from many sources: e.g., departure from Gaussian-harmonic behavior of chains, headgroup interactions, and chemical variations in hydrophobic and other interfacial interactions.

Next, if we accept that the mechanical thickness $h_{pp} - h_o$ is equal to the hydrocarbon thickness, we can use the polymer brush model to predict hydrocarbon thickness and area per lipid $2a$, which can be compared to structural measurements. The simple result is that hydrocarbon thickness and area per molecule depend only on a fixed ratio $c_\gamma = (3k_BT/a_c\gamma)$ of thermal to interfacial energy and the number $n_s = L/2b$ of statistical segments per chain, i.e., $h_{pp} - h_o \approx 2L/(c_\gamma n_s)^{1/3}$ and $2a \approx 0.40$ nm$^2 \times (c_\gamma n_s)^{1/3}$, where $2a_c \approx 0.40$ nm^2 and $L = n_{carbons} \times 0.125$ nm in the all-*trans* configuration. (The polymer brush model also predicts that bending stiffness—scaled by the characteristic energy γL^2—depends uniquely on the ratios c_γ and n_s, i.e., $k_c = (\gamma L^2)/(c_\gamma n_s)^{2/3}$, which yields a range from $k_c \approx 0.57 \times 10^{-19}$ J for C13 to $k_c \approx 1.2 \times 10^{-19}$ J for C22 chains.) Taking the value of $\gamma \approx 40$ mJ/m^2 deduced from the mean stretch modulus defines $c_\gamma \approx 1.5$, so all relations reduce to a simple dependence on the number n_s of statistical segments per chain, i.e., thickness $h_{pp} - h_o \approx 1.75\ L/n_s^{1/3}$ and area per lipid $2a \approx 0.46$ nm$^2 \times n_s^{1/3}$. As shown in the Appendix, correlating the dependence of surface pressure on area per chain predicted by the model to the published

monolayer isotherm for C18:0/1 yields the mean number $L/2b \approx 2.25$ of statistical segments per chain and a persistence length of $b \approx 0.5$ nm. Hence the structural thickness of C18:0/1 is predicted to be $h_{pp} \approx 3.0$ nm + h_o, which agrees with the value in Table 1 if we take $h_o = 1$ nm. Furthermore, assuming common values of persistence length $b \approx 0.5$ nm and $h_o = 1$ nm, thicknesses can be predicted over the full range of chain length from $h_{pp} \approx 3.4$ nm for diC13:0 to $h_{pp} \approx 4.4$ nm for diC22:1, which is again consistent with the span in Table 1. As an experimental comparison for area per molecule, Koenig et al. (1997) used deuterium NMR to derive hydrocarbon thickness and area per lipid by measuring the integrated-average order parameter for ^{2}H-labeled chains. The molecular areas of 0.59 nm^2 for diC14:0 and 0.61 nm^2 for C18:0/1 from their experiments are close to the estimates of 0.55 nm^2 and 0.6 nm^2, respectively, predicted by the polymer brush model.

In contrast to the predictive success for saturated/monounsaturated chain bilayers, neither the thickness nor the bending modulus calculated with the polymer brush relations matches the measured values for bilayers with polyunsaturated chains. Most likely, this stems from increased chain repulsion and peaked stress distributions within the monolayers. For example, a shorter persistence length b could be an origin of larger repulsion between poly-*cis* unsaturated chains. Evidence for this comes from Monte Carlo simulations by Rabinovich and Ripatti (1991), which showed that the mean end-to-end length of a chain diminished as the number of methylene-interrupted *cis* double bonds were increased in a chain. For 18 carbon chains, the apparent increase in chain "flexibility" implied a reduction of ~33% in persistence length. In the context of the polymer brush model, the increase in chain flexibility would reduce the peak-to-peak headgroup thickness by ~0.4 nm to ~3.6 nm for bilayers with C18 chains—again taking h_o = 1 nm. However, even though a 33% reduction in persistence length may account for a large portion of the reduction in thickness, changes in persistence length alone cannot lead to a departure from the linear correlation of elastic ratio to mechanical thickness seen in Fig. 8 for saturated/monounsaturated chain bilayers. This deviation implies a narrowing in the distribution of chain stresses within monolayers of the bilayer or an increase in h_o.

Distributions of chain stresses in PC monolayers have been nicely modeled in recent simulations by Cantor (1999). Invoking the same entropic physics and interfacial energy for hydrocarbon-water interaction as used in our simple theory, Cantor used a mean-field lattice calculation to obtain distributions of lateral stress across monolayers in bilayers. For a wide range of hydrocarbon chain length and unsaturation, the stress distributions resembled flattened half-period sine functions. Generally, monolayers of chains with *cis* double bonds were found to be thinner than layers with saturated chains of the same length. But important asymmetries arose when multiple *cis* bonds appeared at specific locations. In particular, noticeably peaked and asymmetrical distributions were obtained when unsaturated bonds were present near the interface, e.g., C18:1$_{c6}$, C18:3$_{c6,9,12}$, C20:4$_{c5,8,11,14}$, and C22:6$_{c4,7,10,13,16,19}$. It was puzzling, however, that there were essentially no differences in stress distributions or thicknesses between mono- and poly-*cis* unsaturated chains when double bonds started in the nine position, i.e., C18:1$_{c9}$ vis-a-vis C18:3$_{c9,12}$ and C18:3$_{c9,12,15}$, unlike the thickness measurements listed in Table 1. So perhaps a different algorithm is needed to describe the energetics of chain configurations on the lattice in the case of methylene-interrupted *cis* double bonds. As a possible clue, the molecular-model computations of Applegate and Glomset (1991) have shown that angle-iron-shaped conformations of polyene sequences shorten chains significantly, and the reduction in length is larger when polyene sequences are more distal from the water-hydrocarbon interface, as is the case for C18:3$_{c9,12,15}$.

APPENDIX: POLYMER BRUSH MODEL FOR BILAYER ELASTICITY

We use a rudimentary physical model to establish a molecular basis for lateral area compressibility and bending stiffness of a bilayer. The model is based on the premise that surface pressure in a fluid bilayer is dominated by confinement of chain entropy, which neglects van der Waals attraction between chains and specific headgroup interactions. Following Flory (1969), we treat the hydrocarbon chains as short, freely jointed polymers (FJC) characterized by a free energy that depends only on chain extension and the number of statistical segments $n_s = L/2b$—defined by twice the persistence length b. Thus the model provides no information about the distribution of chain stress across the bilayer.

Starting with a flat bilayer, the surface pressure Π in each monolayer is easily derived from the variation of chain free energy F_{ce} with respect to change in hydrocarbon thickness l and area a per chain (Evans and Skalak, 1980),

$$\Pi \cdot \delta a + (\partial F_{ce}/\partial l) \cdot \delta l = 0 \Rightarrow \Pi = -(\partial F_{ce}/\partial l)(\partial l/\partial a) \tag{A1}$$

Assuming constant density, chain packing obeys the requirement that the product $l{\cdot}a$ of hydrocarbon thickness l and area a per chain is a constant $L{\cdot}a_c$ (molecular volume) determined by chain length L and area a_c in the all-*trans* state. Hence surface pressure is derived from the change of chain free energy with chain extension ratio $x = l/L$,

$$\Pi = (x^2/a_c)\partial F_{ce}/\partial x \tag{A2}$$

since $x = a_c/a$ is equivalent to surface density and $(\partial l/\partial a)/L = -(x^2/a_c)$. Introducing the free energy of extension for short FJC polymers, we will use this relation to derive an equation of state for surface pressure and show that it agrees well with a published surface pressure–area isotherm for C18:0/1 (SOPC).

The concept of hydrocarbon chains as freely jointed polymers with long statistical segment lengths is well established from the pioneering work of Flory (1969). For polymethylene polymers of length L, Flory showed that the mean square end-to-end length grows as $\langle r^2 \rangle = 2bL$, as expected for freely jointed chains, but the effective segment (Kuhn) length $2b$ is ~8.3 C-C bonds (i.e., $2b \approx 1$ nm) or about half of the $L \approx 2.25$ nm all-*trans* length of 18 carbon chains. For short chains, Flory also showed that the free energy of extension closely follows a Gaussian-harmonic approximation, $F_{ce} \approx (3n_sk_BT)x^2/2$, up to relatively large extensions (e.g., $x \approx 0.9$ for

$L/2b \approx 4$). By comparison, the free energy for a long polymer begins to diverge logarithmically, i.e., $F_{ce} \approx -n_s k_B T \log_e(1 - x)$, at modest extensions $x > 0.5$. Because hydrocarbon chains in fluid PC bilayers are extended to ~0.7 or less of the all-*trans* length, we can confidently use the harmonic approximation for free energy of chain extension to predict the dependence of surface pressure on area per lipid molecule, which yields

$$\Pi \approx 3n_s(k_B T/a_c)x^3 \approx 3n_s(k_B T/a_c)(a_c/a)^3$$

(For asymmetrical chains with the same all-*trans* area a_c, the ratio $n_s = L/2b$ is defined by $L = (L_1 + L_2)/2$ and $bL = 2(b_1b_2)(L_1L_2)/(L_1b_1 + L_2b_2)$, where subscripts 1 and 2 refer to distinct chains.) We see that surface pressure of a fluid bilayer is expected to decrease as 1/area^3, where the characteristic thermal scale for surface pressure is set by the ratio of temperature to the limiting area per chain, $k_B T/a_c$. To check this, we have correlated the predicted equation of state with the surface pressure-area isotherm measured for C18:0/1 in the liquid-expanded monolayer state in the work of Smaby et al. (1994). Plotted in Fig. 9, we see that the correlation is surprisingly good, given the simplicity of the model. As the only parameter in the correlation, the prefactor $3n_s(k_B T/a_c)$ was found to equal 133 mJ/m^2 at 24°C. Unless characterized by a similar inverse cube dependence on area, there is no evidence of headgroup repulsion at close proximity. Furthermore, Smaby et al. (1994) showed that the limiting area per chain for a wide variety of PCs is $a_c \approx 0.2$ nm^2. This result sets the thermal-surface pressure scale to be $k_B T/a_c \approx 20$ mJ/m^2 (mN/m) at ~20°C. With the surface pressure scale and contour length $L = 2.25$ nm (0.125 nm/carbon × 18), the correlation in Fig. 9 yields $2b = 1$ nm for the effective Kuhn length of the SOPC chains (18:0 and 18:1), which matches Flory's (1969) value for short methylene polymers.

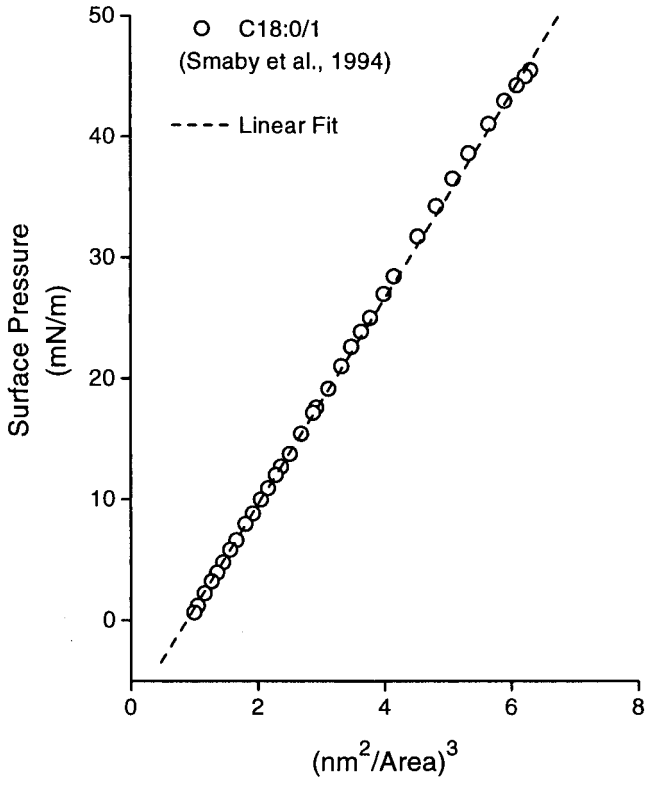

FIGURE 9 Surface pressure-area isotherm of a C18:0/1 PC monolayer in the liquid-expanded state at 24°C, taken from Smaby et al. (1994) and replotted (*open circles*) on a scale defined by the inverse cube of area per lipid (~1/area^3). The solid curve is the chain-entropy model for surface pressure matched by choosing a mean Kuhn length ($2b \approx 1$ nm) for the two (18:0 and 18:1) chains of C18:0/1 PC. The limiting area per chain and chain length for the all-*trans* configuration were taken as $a_c = 0.2$ nm^2 (Smaby et al., 1994) and $L = 18 \times 0.125$ nm $= 2.25$ nm. The polymer brush model predicts that surface pressure should vary as the inverse cube of relative area per chain (i.e., $\Pi \approx (a_c/a)^3$) scaled by the prefactor $3L(k_B T/2a_c b)$, which was found to equal 133 mJ/m^2.

Because surface pressure depends only on chain extension, the elastic area modulus of a bilayer is easily derived to be $K_A = 2x(\partial\Pi/\partial x) \approx 18n_s(k_B T/a_c)x^3$ and thus is determined by monolayer surface pressure ($K_A = 6\Pi$). From thermodynamic minimization of the free energy with respect to lipid surface density, the surface pressure of a monolayer in a flat tension-free bilayer is fixed by the interfacial energy density γ for exposure of hydrocarbon to water, i.e., $\Pi = \gamma$ (Evans and Skalak, 1980; Cantor, 1999). Hence the simple brush model of polymer confinement by hydrophobic interactions predicts that the bilayer surface pressure and elastic area modulus are essentially constants governed by the interfacial energy density γ. Clearly, the energy density γ is affected by chain chemistry (unsaturation, etc.) and interactions in the headgroup region, which will only appear relatively constant for a particular lipid headgroup.

To derive the bending rigidity, we follow the approach used to analyze properties of block copolymer films (Wang and Safran, 1991; Dan and Safran, 1994; Dan, 1999). In contrast to a copolymer film and solution at equilibrium, we assume that the monolayers are kinetically trapped and closed to exchange with the environment or each other, which is appropriate for diacyl lipids. As described above, the energy functional for a monolayer includes the free energy of chain extension plus the interfacial energy associated with hydrophobic interactions,

$$F = \gamma a_i + \varepsilon x^2$$

where a_i is the area per chain at the water-hydrocarbon interface and $\epsilon = 3n_s k_B T/2$ is the harmonic chain energy prefactor. Applying the constraint of constant molecular volume (La_c = constant) to the curved monolayer, chain length l is related to area per molecule a_i at the water-hydrocarbon interface by simple geometry, with curvature as a parameter. The principal curvatures c_1, c_2 describe orthogonal contours embedded in the midsurface of the bilayer, which leads to

$$La_c = a_i l[1 - l(c_1 + c_2)/2 + l^2(c_1c_2)/3]$$

for a monolayer. Next, to simplify derivation of the bending rigidity, the geometry is treated like that of a cylinder ($c_1 = c$ and $c_2 = 0$), and scaled variables are introduced for area, $\underline{a} = a_i/a_c$, and curvature, $\underline{c} = cL$. As such, the packing constraint couples chain extension to curvature and interfacial area,

$$x = (1/\underline{c})[1 - (1 - 2\underline{c}/\underline{a})^{1/2}]$$

Using this relation in the free energy ($F = (\gamma a_c)\underline{a} + \epsilon x^2$) and expanding to quadratic order in curvature, we obtain the approximation

$$F \approx (\gamma a_c)\underline{a} + \varepsilon[1/\underline{a}^2 + \underline{c}/\underline{a}^3 + 5\underline{c}^2/4\underline{a}^4]$$

Minimizing free energy with respect to interfacial area per chain, we establish the relation between interfacial area and curvature, i.e.,

$$\delta F/\delta\underline{a} = 0 \Rightarrow (\gamma a_c) = \varepsilon[2/\underline{a}^3 + 3\underline{c}/\underline{a}^4 + 5\underline{c}^2/\underline{a}^5]$$

Then, introducing a Taylor expansion for $1/\underline{a}$ as a function of curvature, $1/\underline{a} \approx 1/\underline{a}_o + (\cdots)\,\underline{c} + (\cdots)\,\underline{c}^2/2 + \ldots$, and again keeping terms to quadratic order in curvature, we obtain the minimum energy per chain for a cylindrically curved monolayer,

$$F = \varepsilon[3/\underline{a}_o^2 + \underline{c}/\underline{a}_o^3 + \underline{c}^2/2\underline{a}_o^4]$$

where minimization of free energy with respect to surface density sets $1/\underline{a}_o = (\gamma a_c/2\epsilon)^{1/3}$, i.e., $(2\epsilon/a_c)x^3 = 3n_s(k_B T/a_c)x^3 = \gamma$. (This is analogous

to the equilibrium condition $\Pi = \gamma$ for a flat monolayer.) Finally, the free energy per unit area of a cylindrically curved bilayer is found from the sum of upper/lower monolayer energies per unit area. The opposite curvatures of the monolayers eliminate the linear curvature term in the sum of energies to leave a quadratic dependence on curvature,

$$\Sigma_{\pm} F_{\pm}/(a_c \underline{a}_o) = (2\epsilon/a_c)[3x^3 + x^5 \underline{c}^2/2]$$

or equivalently,

$$\Sigma_{\pm} F_{\pm}/(a_c \underline{a}_o) = \gamma[3 + x^2 \underline{c}^2/2]$$

since $(2\epsilon/a_c)x^3 = 3n_s(k_B T/a_c)x^3 = \gamma$. The coefficient of the quadratic term in curvature ($\underline{c}^2 = c^2 L^2$) is the elastic bending stiffness,

$$k_c = (\gamma L^2)x^2$$

where the characteristic energy scale is γL^2. When expressed in terms of the hydrocarbon thickness h and elastic area modulus K_A, the bending stiffness becomes $k_c = K_A h^2/24$. As such, the polymer brush bilayer is two times more rigid than an unbonded pair of isotropic-elastic layers and half as rigid as a bonded pair of isotropic layers—all with the same total thickness.

The authors acknowledge the stimulating and helpful conversations with Myer Bloom at the University of British Columbia (whose curiosity about possible exotic physics in docosahexaenoic acid and its role in brain function motivated this project) and Sid Simon at Duke University (for years of unabridged discussions about unresolved features of membranes).

This work was supported by Medical Research Council grant MT7477 (EE) and National Institutes of Health grants GM40162 (DN), GM08555 (DN), and GM27278 (TM).

REFERENCES

Applegate, K. R., and J. A. Glomset. 1991. Effect of acyl chain unsaturation on the conformation of model diacylglycerols: a computer modeling study. *J. Lipid Res.* 32:1635–1644.

Blaurock, A. E., and C. R. Worthington. 1966. Treatment of low angle x-ray data from planar and concentric multilayered structures. *Biophys. J.* 6:305–312.

Bo, L., and R. E. Waugh. 1989. Determination of bilayer membrane bending stiffness by tether formation from giant thin-walled vesicles. *Biophys. J.* 55:509–517.

Cantor, R. S. 1999. Lipid composition and the lateral pressure profile in bilayers. *Biophys. J.* 76:2625–2639.

Dan, N. 1999. The effect of chain persistence length on the moduli of block copolymer films. *Macromolecules.* 32:1686–1690.

Dan, N., and S. A. Safran. 1994. Self-assembly in mixtures of diblock copolymers. *Macromolecules.* 27:5766–5772.

Duwe, H.-P., H. Englehardt, A. Zilker, and E. Sackmann. 1987. Curvature elasticity of smectic A lipid bilayers and cell plasma membranes. *Mol. Cryst. Liq. Cryst.* 152:1–7.

Evans, E., H. Bowman, A. Leung, D. Needham, and D. Tirrell. 1996. Biomembrane templates for nanoscale conduits and networks. *Science.* 273:933–935.

Evans, E., and D. Needham. 1987. Physical properties of surfactant bilayer membranes: thermal transitions, elasticity, rigidity, cohesion, and colloidal interactions. *J. Phys. Chem.* 91:4219–4228.

Evans, E., and W. Rawicz. 1990. Entropy-driven tension and bending elasticity in condensed-fluid membranes. *Phys. Rev. Lett.* 64: 2094–2097.

Evans, E., and W. Rawicz. 1997. Elasticity of "fuzzy" biomembranes. *Phys. Rev. Lett.* 79:2379–2382.

Evans, E., and R. Skalak. 1980. Mechanics and Thermodynamics of Biomembranes. CRC Press, Boca Raton, FL. 254.

Evans, E., and A. Yeung. 1994. Hidden dynamics in rapid changes of bilayer shape. *Chem. Phys. Lipids.* 73:39–56.

Faucon, J. F., M. D. Mitov, P. Meleard, I. Bivas, and P. Bothorel. 1989. Bending elasticity and thermal fluctuations of lipid membranes: theoretical and experimental requirements. *J. Phys. (Paris).* 50:2389–2414.

Hallett, F. R., J. Marsh, B. G. Nickle, and J. M. Wood. 1993. Mechanical properties of vesicles. II. A model for osmotic swelling and lysis. *Biophys. J.* 64:435–442.

Helfrich, W., and R.-M. Servuss. 1984. Undulations, steric interaction and cohesion of fluid membranes. *Nuovo Cimento.* D3:137–151.

Herbette, L., J. Marquardt, A. Scarpa, and J. K. Blasie. 1977. A direct analysis of lamellar x-ray diffraction from hydrated oriented multilayers of fully functional sarcoplasmic reticulum. *Biophys. J.* 20:245–272.

Hitchcock, P. B., R. Mason, K. M. Thomas, and G. G. Shipley. 1974. Structural chemistry of 1,2 dilauroyl-D,L-phosphatidylethanolamine: molecular conformation and intermolecular packing of phospholipids. *Proc. Natl. Acad. Sci. USA.* 71:3036–3040.

Kim, R. S., and F. S. LaBella. 1987. Comparison of analytical methods for monitoring autoxidation profiles of authentic lipids. *J. Lipid Res.* 28: 1110–1117.

Koenig, B. W., H. H. Strey, and K. Gawrisch. 1997. Membrane lateral compressibility determined by NMR and x-ray diffraction: effect of acyl chain polyunsaturation. *Biophys. J.* 73:1954–1966.

Kwok, R., and E. A. Evans. 1981. Thermoelasticity of large lecithin bilayer vesicles. *Biophys. J.* 35:637–652.

McIntosh, T. J., S. Advani, R. E. Burton, D. V. Zhelev, D. Needham, and S. A. Simon. 1995. Experimental tests for protrusion and undulation pressures in phospholipid bilayers. *Biochemistry.* 34:8520–8532.

McIntosh, T. J., and P. W. Holloway. 1987. Determination of the depth of bromine atoms in bilayers formed from bromolipid probes. *Biochemistry.* 26:1783–1788.

McIntosh, T. J., A. D. Magid, and S. A. Simon. 1987. Steric repulsion between phosphatidylcholine bilayers. *Biochemistry.* 26:7325–7332.

McIntosh, T. J., A. D. Magid, and S. A. Simon. 1989. Cholesterol modifies the short-range repulsive interactions between phosphatidylcholine membranes. *Biochemistry.* 28:17–25.

McIntosh, T. J., and S. A. Simon. 1986a. The hydration force and bilayer deformation: a reevaluation. *Biochemistry.* 25:4058–4066.

McIntosh, T. J., and S. A. Simon. 1986b. Area per molecule and distribution of water in fully hydrated dilauroylphosphatidylethanolamine bilayers. *Biochemistry.* 25:4958–4952.

McIntosh, T. J., S. A. Simon, D. Needham, and C.-H. Huang. 1992. Structure and cohesive properties of sphingomyelin:cholesterol bilayers. *Biochemistry.* 31:2012–2020.

Mui, B. L.-S., P. R. Cullis, E. A. Evans, and T. D. Madden. 1993. Osmotic properties of large unilamellar vesicles prepared by extrusion. *Biophys. J.* 64:443–453.

Needham, D., T. J. McIntosh, and E. A. Evans. 1988. Thermomechanical and transition properties of dimyristoylphosphatidylcholine/cholesterol bilayers. *Biochemistry.* 27:4668–4673.

New, R. R. C. 1990. Liposomes: A Practical Approach. Oxford University Press, Oxford.

Olbrich, K. C., W. Rawicz, D. Needham, and E. Evans. 2000. Water permeability and mechanical strength of polyunsaturated phosphatidylcholine bilayers. *Biophys. J.*

Petrache, H. I., N. Gouliaev, S. Tristram-Nagle, R. Zhang, R. M. Suter, and J. F. Nagle. 1998a. Interbilayer interactions from high-resolution x-ray scattering. *Phys. Rev. E.* 57:7014–7024.

Petrache, H. I., S. Tristram-Nagle and J. F. Nagle. 1998b. Fluid phase structure of EPC and DMPC bilayers. *Chem. Phys. Lipids.* 95:83–94.

Rabinovich, A. L., and P. O. Ripatti. 1991. On the conformational, physical properties and functions of polyunsaturated acyl chains. *Biochim. Biophys. Acta.* 1085:53–62.

Rutkowski, C. A., L. M. Williams, T. H. Haines, and H. Z. Cummins. 1991. The elasticity of synthetic phospholipid vesicles obtained by photon correlation spectroscopy. *Biochemistry.* 30:5688–5696.

Schneider, M. D., J. T. Jenkins, and W. W. Webb. 1984. Thermal fluctuations of large quasi-spherical bimolecular phospholipid vesicles. *J. Phys. (Paris).* 45:1457–1472.

Shannon, C. E. 1949. Communication in the presence of noise. *Proc. Inst. Radio Eng.* 37:10–21.

Smaby, J. M., J. M. Muderhwa, and H. L. Brockman. 1994. Is lateral phase separation required for fatty acid to stimulate lipases in a phosphatidylcholine interface? *Biochemistry.* 33:1915–1922.

Tristram-Nagle, S., H. L. Petrache, and J. F. Nagle. 1998. Structure and interactions of fully hydrated dioleoylphosphatidylcholine bilayers. *Biophys. J.* 75:917–925.

Wang, Z.-G., and S. A. Safran. 1991. Curvature elasticity of diblock copolymer monolayers. *J. Chem. Phys.* 94:679–687.